BLR Physical Conditions in Extreme Population A Quasars: a Method to Estimate Central Black Hole Mass at High Redshift

C. Alenka Negrete and Deborah Dultzin

Instituto de Astonomía, Universidad Nacional Autónoma de México, Mexico

anegrete@astroscu.unam.mx, deborah@astroscu.unam.mx

Paola Marziani

INAF, Astronomical Observatory of Padova, Italy

paola.marziani@oapd.inaf.it

and

Jack W. Sulentic

Instituto de Astrofísica de Andalucía, Spain

sulentic@iaa.es

ABSTRACT

We describe a method for determination of physical conditions in the broad line regions of a significant subsample of Seyfert-1 nuclei and quasars. Several diagnostic ratios based on intermediate (AlIIIλ1860, SiIII]λ1892) and high (CIVλ1549, SiIVλ1397) ionization lines in the UV spectra of quasars are used to constrain density, ionization and metallicity of the emitting gas. We apply the method to two extreme Population A quasars – the prototypical NLSy1 I Zw 1 and a high-z NLSy1-like object, SDSS J120144.36+011611.6. We find well-defined physical conditions: low ionization (ionization parameter $< 10^{-2}$), high density ($10^{12} - 10^{13}$ cm^{-3}) and significant metal enrichment. Ionization parameter and density can be derived independently for each source with an uncertainty that is always less than ± 0.3 in logarithm. We use the product density times ionization parameter to estimate the broad line region radius and the virial black hole mass. Estimates of black hole masses based on the "photoionization" analysis described in this paper are probably more accurate than those derived from the radius – luminosity correlation.

Subject headings: quasars: general — quasars: individual (I Zw 1, SDSS J120144.36+011611.6)

1. Introduction

We lack a simple well-defined diagnostic measure of physical conditions (density, ionization parameter, metallicity) in the broad line region of quasars. Techniques for estimating electron density and ionization in nebular astrophysics (Osterbrock & Ferland 2006) are not straightforwardly applicable to the broad lines of quasars. Reasons include: lines are broad, suitable candidates are too closely spaced in wavelength, and density is at least an order of magnitude higher than the critical density for the forbidden transitions used in spectra of planetary nebulæ and HII regions. The ionization parameter can be estimated from the intensity ratio of two strong resonance lines arising from different ionic stages of the same element. It is again not easy to interpret the results in the case of quasars; for example, where the ratio CIII]λ1909/CIVλ1549 may not yield a meaningful value if the relatively low CIII]λ1909 critical density implies that the the line is formed at larger radii than CIVλ1549. Using lines of different ions introduces additional sources of uncertainty but widens the choice of diagnostic line ratios.

Strong CIII]λ1909 emission implies that $n_{\rm e}$ cannot be very high ($n_{\rm e}\sim$ $10^{11-13}{\rm cm}^{-3}$). However, very high density is invoked to explain the rich low ionization spectrum (especially FeII) seen in quasars. Several lines in the UV spectrum of I Zw 1 (prominent FeII, relatively strong AlIIIλ1860, and CIIIł1176) point towards high density at least for the LIL emitting zone (Baldwin et al. 1996; Laor et al. 1997). This low ionization BLR (or LIL BLR) has very similar properties to the OI and CaII emitting region identified by Matsuoka et al. (2008). The region where these low-ionization lines are produced cannot emit much CIII]λ1909. But is CIII]λ1909 really so strong in most quasars? BLR conditions are certainly complex and a single emitting region is not sufficient to explain both LILs and high ionization lines (HILs).

In this letter we report on an analysis based on several diagnostic ratios used to constrain density, ionization parameter, and metallicity in the BLR of two sources that are representative of relatively large sub-samples of quasars (§2). These sources have the advantage to show weak or no CIII]λ1909 greatly simplifying the interpretation of the emission line spectrum (§3). Diagnostic ratios are heuristically defined (§4) and interpreted through an array of photo-ionization simulations. We show that they converge toward well-defined values of ionization and density (§5). The present analysis can be used to determine the product density times ionization parameter and the distance of the emitting region from the central continuum source $r_{\rm BLR}$ and the virial mass (§6).

2. The sources

The NLSy1 I Zw 1 is an example of the A3 spectral type ($\approx$ 10% of all quasars in the low-z sample of Zamfir et al. 2010). Sources like I Zw 1 are also found at intermediate to high redshift. SDSS J120144.36+011611.6 at $z \approx 3$ is likely a high-redshift, high-luminosity replica of I Zw 1 with broader lines (Fig. 1). Sources of spectral types A3 and A4 are the most extreme Population A quasars (FWHM of Hβ broad component $\lesssim$ 4000 km s^{-1}; Sulentic et al. 2000) in terms of AlIIIλ1860 and FeII emission. If we perform a search in the SDSS DR7 for quasars in the redshift range where both CIV λ1549 and the λ1900 blend are observed at optical wavelengths ($2 \lesssim z \lesssim 3$) we find more than 200 sources out of 3000 candidates with spectra resembling that of I Zw 1 on the basis of AlIIIλ1860 strength.

3. Analysis of the Emission Line Spectrum

FeIII lines are common and strong in the vicinity of CIII]λ1909 as seen in the SDSS template quasar spectrum (Vanden Berk et al. 2001). They appear to be strong when AlIIIλ1860 is also strong (Hartig & Baldwin 1986). We adopt the template (option B) of Vestergaard & Wilkes (2001) for modeling FeIII emission in our sources. Lyα pumping enhances FeIII (UV 34)ł1914.0 (Johansson et al. 2000) and this line can be a major contributor to the blend on the red side of CIII]λ1909. The spectrum of I Zw 1 convincingly demonstrates this effect: both CIII]λ1909 abd FeIII (UV 34)ł1914.0 are needed to account for the double peaked feature at 1910 Å that is too broad to be explained by a single line (Fig. 1).[1] The UV FeII template we adopt (FeII is not very strong in the spectral range we analyze) is based on a suitable CLOUDY simulation.

The SPECFIT IRAF task (Kriss 1994) allows us to fit the continuum, emission and absorption line components, as well as FeII and FeIII contributions. We used the same power-law to describe the continuum at both the CIVλ1549 and 1900Å regions. We checked that the SPECFIT solution properly accounted for the FeII UV 191 multiplet and the FeIII features at 1930 and 2080 Å that are unblended with other lines.

The SPECFIT routine permits the deconvolution of SiIII]λ1892, making the AlIIIλ1860/SiIII]λ1892 ratio reliable. In Pop. A low (SiIIλ1814) and intermediate ionization (AlIIIλ1860, SiIII]λ1892) lines (IILs) offer the key advantage of showing only the core broad component (BC) associated to low-ionization emission; HILs (CIVλ1549 and SiIVλ1397) are decomposed into a

[1]Note that the Galactic line of Mg I at 2026 Å can contribute to the split appearance of the redshifted λ1910 Å feature (Fig. 1). This absorption line is included in our `specfit` analysis.

Lorentzian BC with the same width and shifts of the IILs plus a blueshifted residual (assumed to be Gaussian in the SPECFIT procedure; Marziani et al. 2010).

A second key advantage of the extreme Pop. A sources is that CIII]λ1909 is weak or even absent (Fig. 1). The fit to SDSS J120144.36+011611.6 suggests almost no CIII]λ1909 emission if enhanced FeIII ł1914 is included. If FeIII ł1914 is removed a maximum CIII]λ1909 contribution is ≈ 0.4 SiIII]λ1892 and the fit cannot model the red side of the blend. CIII]λ1909 emission in I Zw 1 is about ≈ 0.6 SiIII]λ1892.

The very dense region emitting the LILs should produce no CIII]λ1909; so any emission from this line should arise in a different region. Reverberation mapping data for NGC 5548 suggest that CIII]λ1909 is mainly emitted farther from the central continuum source than Hβ (Peterson et al. 2004). There are also plausible physical scenarios that can give rise to CIII]λ1909 in a shielded, non-uniform environment (Maiolino et al. 2010). Since we are considering profiles integrated over the whole unresolved emitting region, the relevant question is: how much will the CIII]λ1909 emitting regions contribute to the lines we are considering? The strongest CIII]λ1909 emitters along the E1 sequence (spectral type A1) typically show SiIII]λ1892/CIII]λ1909 ≈ 0.4 Kuraszkiewicz et al. (2004). Other IILs will be less affected. If the ionization parameter is $\log U \lesssim -2.5$, there will be also modest HIL emission. What we have estimated here is in many ways the maximum CIII]λ1909 emission that we find weak. We therefore neglect the effect of any CIII]λ1909 emitting gas on the IILs.

4. Diagnostic ratios and their interpretation

Figure 2 (left panel) shows the ionic fraction as a function of the geometrical depth in a slab of fixed column density ($N_{\rm c}$= 10^{25} cm^{-2}) and density ($n_{\rm H}$= $10^{12.5}$cm^{-2}) exposed to a standard quasar continuum. Al^{++}, Fe^{++}, and Si^{++} share a region of dominance deep in the cloud, close to the end of the Strömgren sphere where the HILs are also emitted. It is very appropriate to consider IIL ratios since IILs are emitted in the same zones within the slab (right panel of Figure 2).

Line ratios like AlIIIλ1860/SiIII]λ1892 are useful diagnostics over a range of density that depends on their transition probabilities. Emission lines originating from forbidden or semi-forbidden transitions become collisionally quenched above the critical density and, hence, weaker than lines for which collisional effects are still negligible. The AlIIIλ1860/SiIII]λ1892 ratio is well suited to sample the density range $10^{11} - 10^{13}$ cm^{-3}. This corresponds to the densest, low ionization emitting regions likely associated with the production of FeII.

The ratios SiII]λ1814 /SiIII]λ1892 and SiIVλ1397/ SiIII]λ1892 are sensitive to ionization, but roughly independent of metallicity. Conversely the ratio CIV λ1549/SiIV λ1397 is mainly sensitive to [Si/C].

We computed a multidimensional grid of CLOUDY simulations to derive estimates of U and $n_{\rm H}$ from our spectral measurements (Ferland et al. 1998; Korista et al. 1997). CLOUDY computes population levels of the relevant ionic stages of Si, C, Al and, especially for lines emitted in the fully ionized part of the slab (Fig. 2), is expected to predict reliable relative line intensities. Simulations span the density range $7.00 \leq \log n_{\rm H} \leq 14.00$, and $-4.50 \leq \log U \leq 00.00$, in intervals of 0.25 assuming of plane-parallel geometry. We considered three chemical compositions: (1) solar metallicity: (2) constant solar abundance ratio Al:Si:C with $Z = 5Z_{\odot}$ (5Z); (3) an overabundance of Si and Al with respect to carbon by a factor 3, again with $Z = 5Z_{\odot}$ (5ZSA). This last condition comes from the yields listed for type II Supernovæ (Woosley & Weaver 1995).

5. Results

Table 1 reports the fluxes of the BC for IILs and HILs. We compute the ratios analyzed above from these values. They are shown as constant value contours in the U vs. $n_{\rm H}$ plane obtained from `cloudy` simulations. At first, we assume metallicity equal to solar (Fig. 3, left panels). There is convergence towards a low ionization plus high density range.

The discrepancy in the intersection point is significant for the SiIVλ1397/CIVλ1549 ratio that depends mainly on the Si abundance relative to C.

In equivalent plots made for $Z = 5Z_{\odot}$SA, the agreement improves (Fig. 3). High metallicity yields higher U and smaller $n_{\rm H}$ if emission line ratios involving CIVλ1549 are considered. This reflects the increase in abundance of Si and Al relative to C, and the fact the SiIIλ1814, SiIII]λ1892, AlIIIλ1860 lines are emitted at lower ionization than CIVλ1549. The Si overabundance is also expected in the chemical composition of gas returned to the interstellar medium by an evolved population with a top-loaded initial mass function simulated using STARBURST 99 (Leitherer et al. 1999). Independent evidence based on the strength of NVλ1240 relative to CIVλ1549 and HeIIλ1640 indicates that chemical abundances may be 5 to 10 times solar (Dhanda et al. 2007) in high redshift quasars, with Z $\approx 5Z_{\odot}$ reputed typical of high z quasars (Ferland et al. 1996).

The halftone bands also show that we underestimate SiIIλ1814 somewhat. SiIIλ1814 is the only low-ionization line considered in this study, and its formation is sensitive to the assumed X-ray continuum. IILs and HILs bypass the problem of LIL formation and offer

results consistent with a well-defined value of U and $n_{\rm H}$.

6. Implications

The ionization parameter U and $n_{\rm H}$ are related to $r_{\rm BLR}$ through the equation $r_{\rm BLR} = \mathrm{const}\, Q^{\frac{1}{2}}(U n_{\rm H})^{-\frac{1}{2}}$ where Q is the number of H-ionizing photons. The dependence of U on $r_{\rm BLR}$ was used to derive central black hole masses assuming a plausible average value of the product $n_{\rm H}{\cdot}U$ and using the Hβ width as a virial broadening estimator (Padovani et al. 1990; Wandel et al. 1999).

Using our derivations for $n_{\rm H}$ and U, we obtain $r_{\rm BLR}$ and $M_{\rm BH}$ values listed in Table 2. Asymmetric errors have been quadratically propagated following Barlow (2004). The last columns give the virial black hole masses following our method and using the $r_{\rm BLR}$ – luminosity correlation (Vestergaard & Peterson 2006). The large intrinsic dispersion of the $r_{\rm BLR}$ – luminosity relation (± 0.66 at a 2σ confidence level) and its uncertain extrapolation makes the "photoionization" method presented here more appropriate for estimating $M_{\rm BH}$ in high-z quasars.

7. CONCLUSION

Diagnostics for density ionization and metallicity is possible for NLSy1-like sources at high redshift. Accurate diagnostics require high S/N and moderate dispersion but in principle can be applied to very high z (> 6.5) using data from IR spectrometers. The product $(n_{\rm H}U)$ yields the possibility of deriving $r_{\rm BLR}$ and $M_{\rm BH}$ for a significant number of sources. Negrete et al. (2011, in preparation) will present an analysis of the applicability of the photoionization method described here to the general population of quasars.

REFERENCES

Baldwin, J. A., et al. 1996, ApJ, 461, 664

Barlow, R. 2004, ArXiv Physics e-prints, arXiv:physics/0406120

Dhanda, N., Baldwin, J. A., Bentz, M. C., & Osmer, P. S. 2007, ApJ, 658, 804

Ferland, G. J., Baldwin, J. A., Korista, K. T., Hamann, F., Carswell, R. F., Phillips, M., Wilkes, B., & Williams, R. E. 1996, ApJ, 461, 683

Ferland, G. J., Korista, K. T., Verner, D. A., Ferguson, J. W., Kingdon, J. B., & Verner, E. M. 1998, PASP, 110, 761

Hartig, G. F., & Baldwin, J. A. 1986, ApJ, 302, 64

Johansson, S., Zethson, T., Hartman, H., Ekberg, J. O., Ishibashi, K., Davidson, K., & Gull, T. 2000, A&Ap, 361, 977

Korista, K., Baldwin, J., Ferland, G., & Verner, D. 1997, ApJS, 108, 401

Kriss, G. 1994, Astronomical Data Analysis Software and Systems III, A.S.P. Conference Series, 61, 437

Kuraszkiewicz, J. K., Green, P. J., Crenshaw, D. M., Dunn, J., Forster, K., Vestergaard, M., & Aldcroft, T. L. 2004, ApJS, 150, 165

Laor, A., Jannuzi, B. T., Green, R. F., & Boroson, T. A. 1997, ApJ, 489, 656

Leitherer, C., et al. 1999, ApJS, 123, 3

Maiolino, R., et al. 2010, A&A, 517, A47+

Marziani, P., Sulentic, J. W., Negrete, C. A., Dultzin, D., Zamfir, S., & Bachev, R. 2010, MNRAS, 409, 1033

Matsuoka, Y., Kawara, K., & Oyabu, S. 2008, ApJ, 673, 62

Osterbrock, D. E., & Ferland, G. J. 2006, Astrophysics of gaseous nebulae and active galactic nuclei (University Science Books)

Padovani, P., Burg, R., & Edelson, R. A. 1990, ApJ, 353, 438

Peterson, B. M., et al. 2004, ApJ, 613, 682

Sulentic, J. W., Marziani, P., & Dultzin-Hacyan, D. 2000, ARA&A, 38, 521

Vanden Berk, D. E., et al. 2001, AJ, 122, 549

Vestergaard, M., & Peterson, B. M. 2006, ApJ, 641, 689

Vestergaard, M., & Wilkes, B. J. 2001, ApJS, 134, 1

Wandel, A., Peterson, B. M., & Malkan, M. A. 1999, ApJ, 526, 579

Woosley, S. E., & Weaver, T. A. 1995, ApJS, 101, 181

Zamfir, S., Sulentic, J. W., Marziani, P., & Dultzin, D. 2010, MNRAS, 403, 1759

This preprint was prepared with the AAS LaTeX macros v5.2.

Table 1. Measured quantities

Object	z	f_λ(1700 Å)[a]	SiIVλ1397[b]	CIVλ1549[b]	SiIIλ1814[b]	AlIIIλ1860[b]	SiIII]λ1892[b]	CIII]λ1909[b]	FWHM[c]
I Zw 1	0.0605	3.1	19.3±4.0	$27.0^{+8.0}_{-3.0}$	$3.5^{+2.5}_{-1.0}$	16.6±3.3	31.1±6.2	18.0±3.6	1050±100
SDSS J1201+0116	3.2332	1.6	12.9±2.6	$15.0^{+4.5}_{-1.5}$	$3.0^{+2.0}_{-1.5}$	11.2±2.2	11.0±2.2	3.0:	4000±400

[a]Rest-frame specific flux in units of 10^{-14} erg s^{-1} cm^{-2} Å^{-1}.

[b]Rest-frame flux in units of 10^{-14} erg s^{-1} cm^{-2}.

[c]Rest frame FWHM of IIL line BC and of the CIVλ1549 BC in units of km s^{-1}.

Table 2. Derived quantities

Object	$\log n_{\rm H}$[a]	$\log U$	$\log(n_{\rm H}U)$	$\log r_{\rm BLR}$[b]	$\log M_{\rm BH}$[c]	$\log M_{\rm BH}$(VP06)[d]
I Zw 1	$12.05^{+0.15}_{-0.30}$	$-2.65^{+0.40}_{-0.15}$	$9.4^{+0.4}_{-0.3}$	$17.29^{+0.22}_{-0.18}$	$7.09^{+0.23}_{-0.20}$	6.70
SDSS J1201+0116	$12.75^{+0.3}_{-0.15}$	$-3.00^{+0.15}_{-0.10}$	$9.75^{+0.3}_{-0.2}$	$18.37^{+0.14}_{-0.17}$	$9.33^{+0.19}_{-0.17}$	9.29

[a]$n_{\rm H}$ in units of cm^{-3}.

[b]$r_{\rm BLR}$ in units of cm.

[c]$M_{\rm BH}$ in units of M$_\odot$ computed using the customary virial formula $M_{\rm BH}= f r_{\rm BLR}{\rm FWHM}^2/G$, with the FWHM values of Tab. 1, and $f = 0.75$.

[c]$M_{\rm BH}$ in units of M$_\odot$ computed following Vestergaard & Peterson (2006), and input parameters reported in note (b).

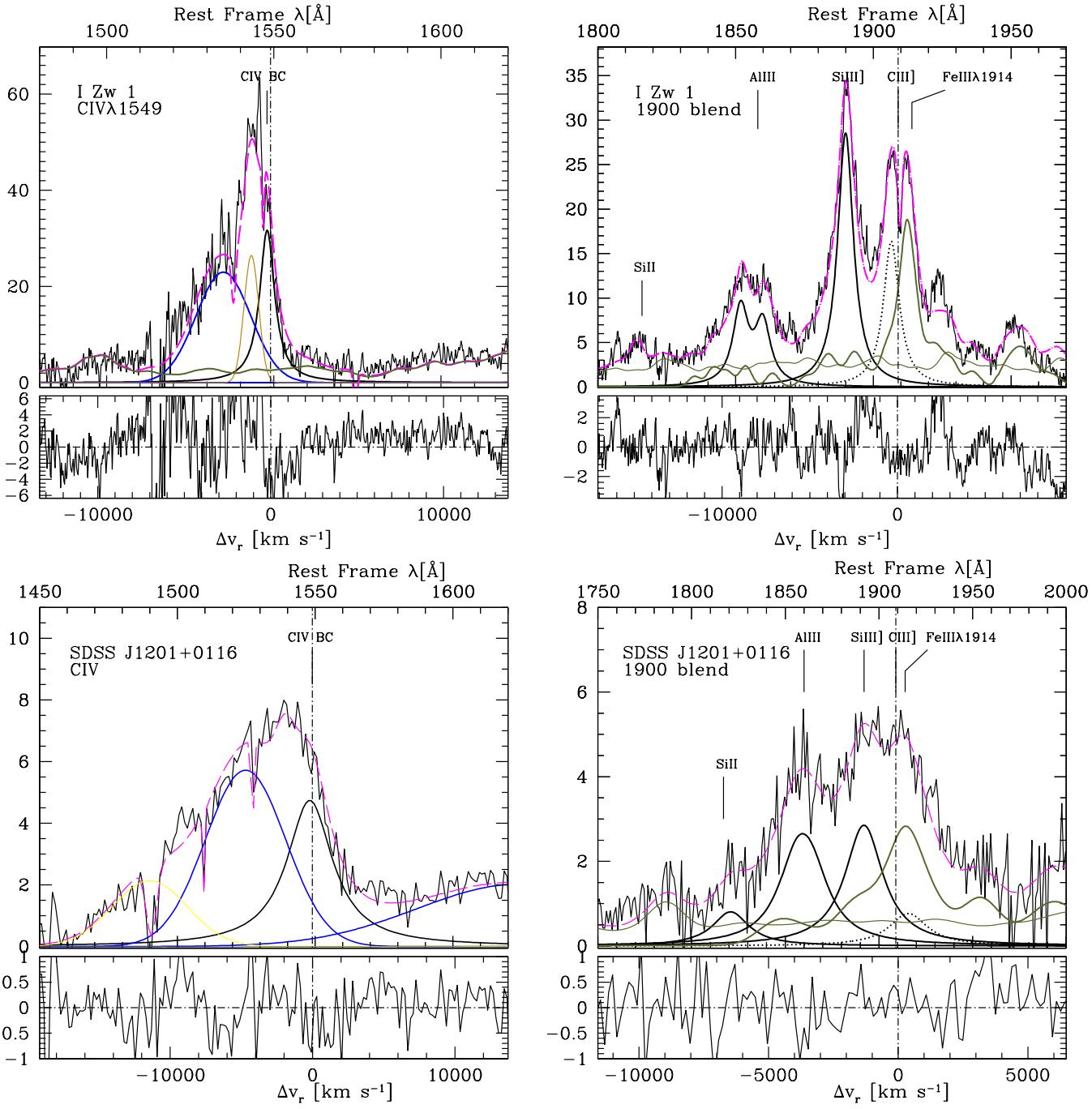

Fig. 1.— CIV λ 1549 (left) and λ1900 spectral region (right) of I Zw 1 (top) and SDSS J120144.36+011611.6. The vertical scale is rest-frame specific flux in units of ergs s^{-1} cm^{-2} $Å^{-1}$. The major constituents of the blend are AlIIIλ1860, SiIII]λ1892, FeIII. The thin olive line represents template FeII emission, the thick one FeIII. The dotted line corresponds to the CIII]λ1909 estimated contribution. See text for details.

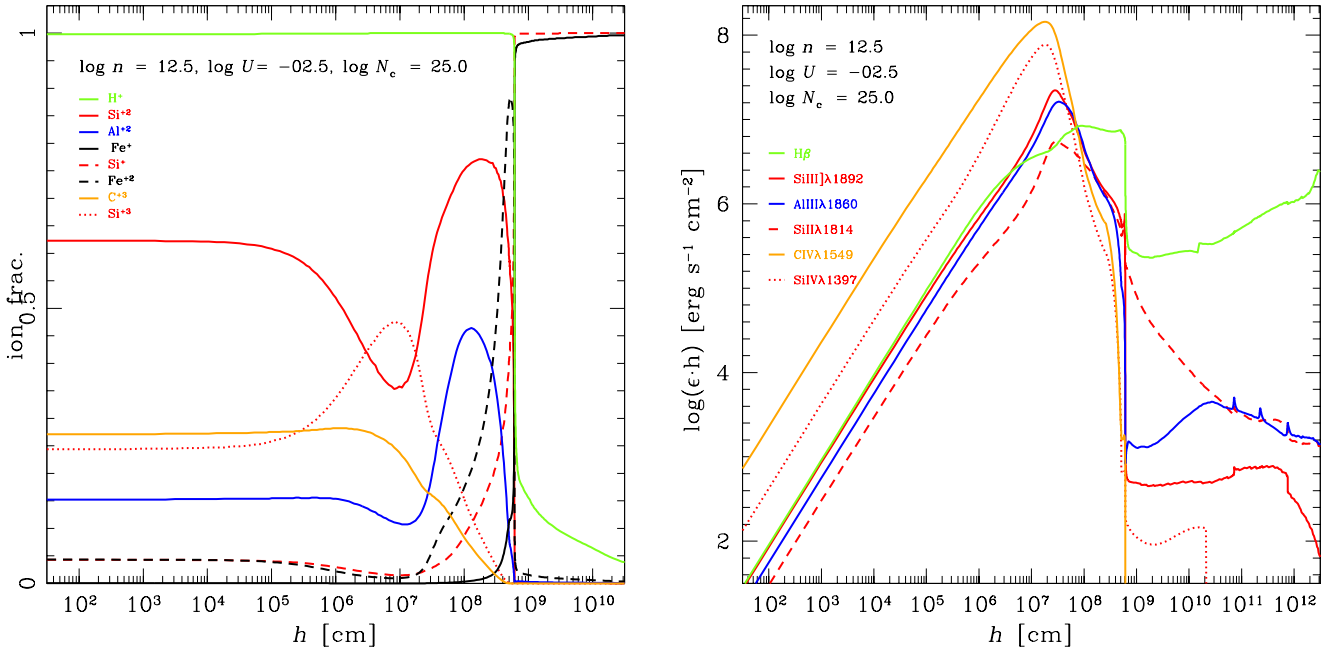

Fig. 2.— Left: Ionic Fractions as a function of the geometric depth h in the gas slab. Right: Line emissivity per unit volume in units of ergs s^{-1} cm^{-3} multiplied by depth h in cm.

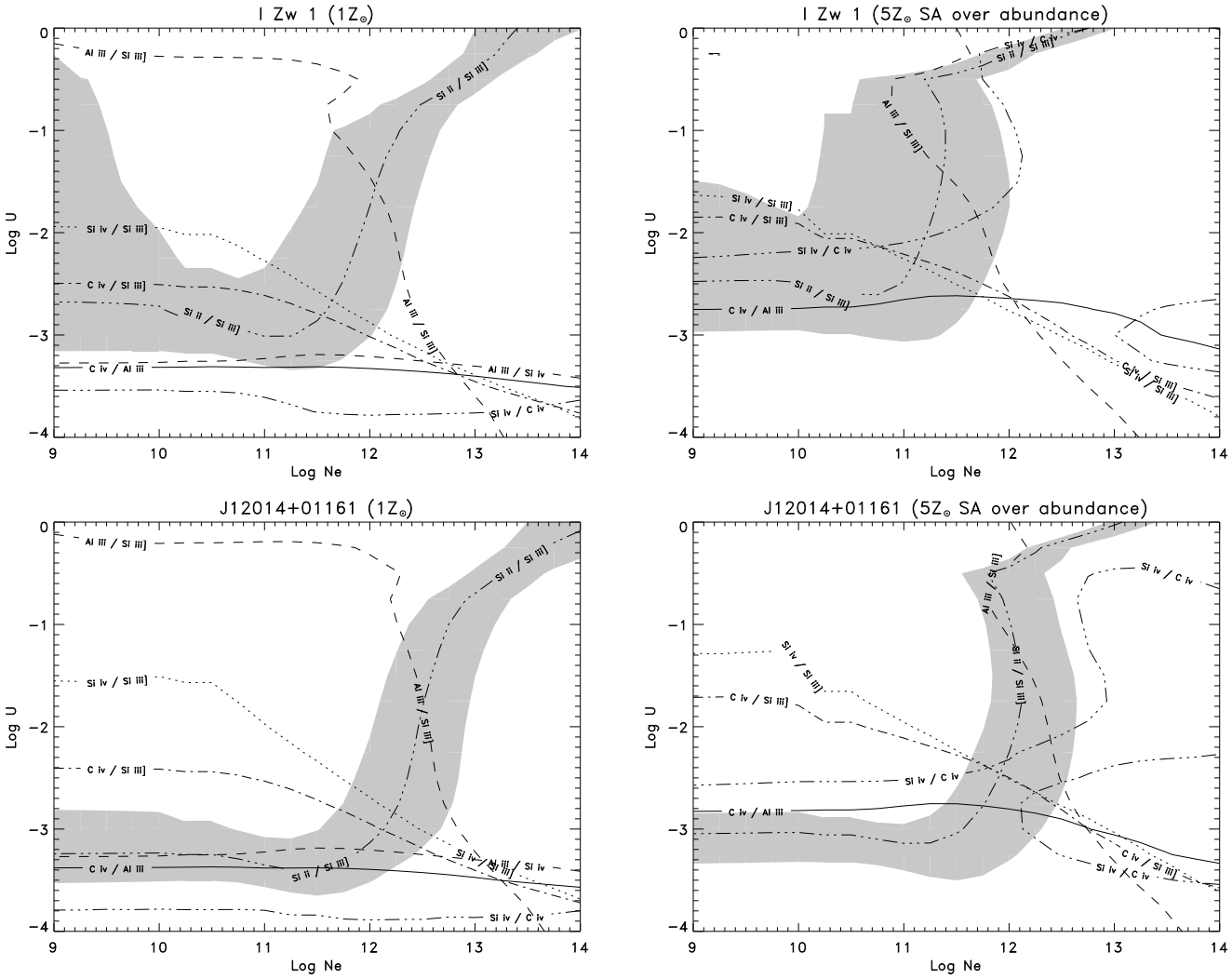

Fig. 3.— Iso-contour of diagnostic ratios for I Zw 1 (top) and SDSS J120144.36+011611.6 (bottom). The left panels refer to the case of solar metallicity; the right ones to the case of five times solar plus a factor of three metal enrichment (5ZSA). The grey band is the uncertainty band of the ratio SiIIλ1814/SiIII]λ1892. Note that the SiIVλ1397/CIVλ1549 is not proving a useful constraint in the 5ZSA case since it varies little in a wide area around the intersection point in the (U,$n_{\rm H}$) plane.